LES of canonical shock-turbulence interaction

By I. Bermejo-Moreno, J. Larsson AND S. K. Lele

1. Motivation and objective

The interaction between shock waves and turbulence is present in a large variety of high-speed flows with relevance in scientific and engineering applications. The use of large-eddy simulations (LES) to predict such flows requires subgrid-scale (SGS) models capable of accurately representing the physics behind this interaction at the unresolved scales. The canonical shock-turbulence interaction problem, consisting of isotropic turbulence passing through a nominally normal shock, isolates the fundamentals of this mutual interaction and can be considered a good benchmark case to test the performance of SGS models.

The problem of shock-turbulence interaction has been studied theoretically (Ribner 1953; Lee *et al.* 1992; Lele 1992; Jacquin *et al.* 1993; Wouchuk *et al.* 2009), experimentally (Hesselink & Sturtevant 1988; Keller & Merzkirch 1990; Barre *et al.* 1996; Agui *et al.* 2005) and numerically, both through direct numerical simulations (DNS) (Lee *et al.* 1993, 1997; Hannappel & Friedrich 1995; Mahesh *et al.* 1997; Larsson & Lele 2009) and LES (Lee 1992; Ducros *et al.* 1999). LES of the canonical case are nonetheless scarce in the literature, compared, for example, with LES of the shock-boundary layer interaction.

The aim of the present work is to compare the performance of several SGS models for LES of the canonical shock-turbulence interaction problem, focusing on the region immediately downstream of the shock, which poses most of the modeling challenges (Bermejo-Moreno 2009). DNS results obtained following Larsson & Lele (2009) will be used for comparison. Section 2 describes the mathematical formulation, geometric configuration and numerical method used in this study. The SGS models implemented for comparison are introduced in Section 3. We propose in Section 4 a conditional application of the SGS model that avoids adding SGS dissipation to flow regions where excessive numerical dissipation is expected. LES results are presented in Section 5 for different flow conditions and compared with filtered DNS data, also evaluating the influence of the grid resolution, numerical scheme and conditional SGS application. Conclusions and future plans are presented in Section 6.

2. Mathematical formulation, computational domain and numerical method

The following LES formulation for conservation of mass, momentum and total energy is considered:

$$\partial_t \overline{\rho} + \partial_j(\overline{\rho}\widetilde{u}_j) = 0 \tag{2.1}$$

$$\partial_t(\overline{\rho}\widetilde{u}_i) + \partial_j(\overline{\rho}\widetilde{u}_i\widetilde{u}_j) = -\partial_j\overline{p} + \partial_j\check{d}_{ij} - \partial_j\tau^S_{ij} \tag{2.2}$$

$$\partial_t(\overline{\rho}\widetilde{e}_T) + \partial_j(\overline{\rho}\widetilde{e}_T\widetilde{u}_j) = -\partial_j(\overline{p}\widetilde{u}_j) + \partial_j(\check{d}_{ij}\widetilde{u}_i) - \partial_j\check{q}_j - c_p\partial_j q^S_j, \tag{2.3}$$

where ρ is the density, t the time, u_i the velocity component in the x_i-direction, p the thermodynamic pressure, T the temperature and e_T the total energy. For a flow variable

f, $\overline{f}$ denotes the LES filtering operation, $\widetilde{f} = \overline{\rho f}/\overline{\rho}$ is the Favre (density-averaged) quantity, and $\check{f}$ refers to the formal expression of f with all constituent variables replaced with their Favre-filtered counterparts: $\check{d}_{ij} \equiv d_{ij}(\widetilde{T}, \widetilde{\mathbf{u}}) \equiv \mu(\widetilde{T})\,[(\partial_j \widetilde{u}_i + \partial_j \widetilde{u}_j) - (2/3)\partial_k \widetilde{u}_k \delta_{ij}]$, and $\check{q}_j \equiv q_j(\widetilde{T}) \equiv \kappa(\widetilde{T})\partial\widetilde{T}/\partial x_j$. The shear viscosity is given by a power law of temperature, $\mu(T) = \mu_0(T/T_0)^{3/4}$ and the thermal conductivity, κ, is related to the viscosity through a constant Prandtl number, Pr: $\kappa(T) = c_p\mu(T)/Pr$, where c_p is the heat capacity at constant pressure. The bulk viscosity has been considered nil. The differential equations are completed with the equation of state for an ideal gas: $\overline{p} = R\,\overline{\rho}\widetilde{T}$, where R is the specific gas constant. The modeling terms considered in this study are the SGS stress tensor, τ_{ij}^S (both its trace and deviatoric part), the SGS heat flux, q_j^S, and the SGS pressure-velocity correlation term, which, for the total energy equation, can be reformulated in terms of the SGS heat flux as $\overline{pu_j} - \overline{p}\widetilde{u}_j = Rq_j^S$, by using the equation of state, as already accounted for in Equation (2.3) through the c_p coefficient pre-multiplying the divergence of SGS heat flux. Other modeling terms (see Bermejo-Moreno 2009), such as the SGS turbulent diffusion and the SGS viscous diffusion, are neglected.

The computational domain is a rectangular box of dimensions $3\pi \times (2\pi)^2$ in the streamwise (x) and transverse (y, z) directions. The equations are numerically solved using a finite-difference methodology. A solution-adaptive, hybrid approach is utilized to numerically approximate the inviscid fluxes. It combines a seventh-order accurate weighted essentially non-oscillatory (WENO) scheme near shock waves with a sixth-order accurate central-difference scheme, on the split form of Ducros *et al.* (2000), elsewhere. Shock waves are identified by means of the sensor $s = -\partial_j u_j/(|\partial_j u_j| + \langle\omega_j\omega_j\rangle_{YZ}^{1/2})$, where $\langle\cdot\rangle_{YZ}$ is the instantaneous average on transverse planes and ω_i is the vorticity. WENO is only applied in the streamwise direction, for grid points where $s > 0.6$. The same sixth-order central difference scheme is applied to the viscous terms everywhere. Integration in time is accomplished through a fourth-order Runge-Kutta method.

The inflow turbulence is generated by means of an independent DNS of isotropic decaying turbulence with an initial von Kármán spectrum that peaks at a wavenumber $k = k_0 = 6$. To ensure that the turbulence is fully developed, the DNS is allowed to decay for approximately three eddy-turnover times. After the decay, the Taylor microscale Reynolds number is $Re_\lambda \approx 75$. The LES resolutions chosen for this study ensure that the cutoff wavenumber lies within the inertial range of the DNS. This inflow turbulence is then top-hat filtered to the LES resolution and advected with a uniform streamwise velocity at the inlet of the LES domain, resulting in a mean Mach number of the incoming flow of $M = 1.5$. A second case with $M = 3.5$ will be also considered. The turbulent Mach number (defined as the ratio between the turbulent kinetic energy and the sound speed) at the inlet in both cases is $M_t = 0.16$. The shock location is stationary in time on average, by imposing a mean back pressure at the outlet (see Larsson & Lele 2009). A sponge layer extends $2\pi/3$ upstream from the outlet, to prevent propagation of spurious reflections of acoustic waves at the outflow boundary back into the computational domain, since the flow downstream of the shock is subsonic. Periodic boundary conditions apply in the transverse directions.

3. Subgrid-scale models implemented

Two classes of SGS models are implemented: mixed eddy-diffusivity and structure-based models. The former assumes that the effect of turbulent subgrid scales can be represented by a gradient diffusion law through an appropriate eddy diffusivity, possibly

SGS quantity	ζ	η	$\mathcal{G}$	c_e
Kinetic energy, $K^S = \frac{1}{2}\tau_{ii}^S$	τ_{ii}^S	u_i	$2\lvert\widetilde{S}\rvert$	C_I
Deviatoric stress tensor, $\tau_{ij}^S - \frac{1}{3}\tau_{kk}^S\delta_{ij}$	τ_{ij}^S	u_j	$-2\widetilde{S}_{ij}$	C
Heat flux	q_i^S	T	$-\partial\widetilde{T}/\partial x_i$	C/Pr_t

TABLE 1. Modeled SGS quantities; associated η variable; eddy-diffusivity functional dependence, $\mathcal{G}$; coefficients, c_e.

complemented with an additional term (e.g., based on scale invariance), whereas the latter assumes the SGS motion to be produced by an ensemble of coherent structures from which the closure terms are derived.

3.1. *Mixed eddy-diffusivity models*

For a general SGS closure term $\zeta = \overline{\rho}(\widetilde{u_i\eta} - \widetilde{u}_i\widetilde{\eta})$, where $\eta(\mathbf{x}, t)$ is a flow variable that will be later particularized for each (scalar, vectorial or tensorial) quantity ζ to be modeled (see Table 1), a mixed eddy-diffusivity model assumes the form $\zeta^{\text{model}} = \mathcal{MT} + \mathcal{ED}$, where $\mathcal{ED}$ is an eddy-diffusivity term and $\mathcal{MT}$ is the mixed term.

The eddy-diffusivity term is expressed as $\mathcal{ED} = \overline{\rho}\nu_e(u_i)\mathcal{G}(\widetilde{\eta})$, where $\nu_e(\widetilde{u}_i) = c_e\vartheta(\widetilde{u}_i)$ is the eddy diffusivity that depends on the resolved velocity field through a function $\vartheta(\widetilde{u}_i)$, and incorporates the model coefficient, c_e. The function $\mathcal{G}(\widetilde{\eta})$ mimics the corresponding physical diffusion law (typically of the form of a turbulent gradient) for the modeled quantity (see Table 1). Two different forms of eddy diffusivity are considered in this study: Smagorinsky's version (Smagorinsky 1963) is based on the assumption of a Newtonian-viscous-like SGS stress tensor, dimensional analysis and a simplified balance of turbulent kinetic energy between production and dissipation that neglects convective and diffusive terms, resulting in $\vartheta^{\text{Smag}} = \Delta^2|\widetilde{S}|$, where $|\widetilde{S}| \equiv (2\widetilde{S}_{ij}\widetilde{S}_{ij})^{1/2}$, $\Delta = (\Delta_1\Delta_2\Delta_3)^{1/3}$ and Δ_i is the local grid spacing in the x_i-direction; Vreman's version (Vreman 2004) is based on the second invariant, II_β, of the tensor $\beta_{ij} = \Delta_k^2\partial_i\widetilde{u}_k\partial_j\widetilde{u}_k$, whose collection of all local flow types with n zero velocity derivatives ($n \in [0, 9]$) equals that of the theoretical SGS dissipation, $-\tau_{ij}^S\widetilde{S}_{ij}$. By adding a realizability condition and imposing the correct behavior at the wall ($\nu_e = 0$), it is obtained $\vartheta_e^{\text{Vrem}} = [II_\beta/(\partial_j\widetilde{u}_i\partial_j\widetilde{u}_i)]^{1/3}$.

Three alternative mixed terms, $\mathcal{MT}$, are considered. The first option assumes a nil term, $\mathcal{MT}_1 \equiv 0$, obtaining a purely eddy-diffusivity model. In the other two alternatives, the closure term ζ is expanded in Galilean-invariant components, one of which, the Leonard term $\mathcal{L} = \overline{\rho}(\widetilde{\widetilde{u}_i\widetilde{\eta}} - \widetilde{\widetilde{u}}_i\widetilde{\widetilde{\eta}})$, is modeled by the mixed term. The *gradient mixed-term* approach uses a Taylor series expansion of the Leonard term, assuming that the Favre-filter can be approximated by either a Gaussian or a top-hat filter, resulting in the form $\mathcal{MT}_2 = \overline{\rho}\Delta_k^2\widetilde{u}_{i,k}\eta_{,k}/12$. The *similarity mixed-term* approach approximates the unknown Favre-filter by an assumed numerical low-pass filter, $\mathcal{F}$, computing the Leonard term directly as $\mathcal{MT}_3 = \overline{\rho}(\widetilde{\widetilde{u}_i\widetilde{\eta}} - \widetilde{\widetilde{u}}_i\widetilde{\widetilde{\eta}}) \approx \overline{\rho}[\mathcal{F}(\widetilde{u}_i\widetilde{\eta}) - \mathcal{F}(\widetilde{u}_i)\mathcal{F}(\widetilde{\eta})]$.

The model coefficient, c_e, is dynamically calculated following Germano's procedure (Germano *et al.* 1991), by means of a test-filter, denoted by $\widehat{(\cdot)}$, which is applied on the resolved flow variables. It is assumed that the same model form and model coefficient apply at the resolved and test-filtered scales and that the variation of c_e within the test-filter width is negligible compared to that of $\chi \equiv \overline{\rho}\vartheta(\widetilde{u}_i)\mathcal{G}(\eta)$, obtaining

$$\Lambda \equiv \zeta^L - (\mathcal{MT}^T - \widehat{\mathcal{MT}}) = c_e(\chi^T - \widehat{\chi}) \equiv c_e\Upsilon, \tag{3.1}$$

where $\zeta^L \equiv \widehat{\overline{\rho}\widetilde{u}_i\widetilde{\eta}} - \widehat{\overline{\rho}\widetilde{u}_i}\widehat{\overline{\rho}\widetilde{\eta}}/\widehat{\overline{\rho}}$, $\mathcal{M}\mathcal{T}^T \equiv \widehat{\overline{\rho}}(\widehat{\widetilde{u}_i\widetilde{\eta}} - \widehat{\widetilde{u}}_i\widehat{\widetilde{\eta}})$, $\chi^T \equiv \widehat{\overline{\rho}}\vartheta(\widehat{\widetilde{u}}_i)\mathcal{G}(\widehat{\widetilde{\eta}})$. Then, c_e can be determined by minimizing (in a least-squares sense that follows Lilly 1992) the total error in a given domain Ω, $E \equiv \int_\Omega (\Lambda - c_e\Upsilon)^2 W \mathrm{d}\Omega$: $\delta E/\delta c_e = 0 \Rightarrow c_e = I_{\Lambda\Upsilon}/I_{\Upsilon\Upsilon}$, where $I_{AB} = \int_\Omega ABW_e \mathrm{d}\Omega$ and W is a weighting function defined in Ω, which can be spatial and/or temporal. Different choices of Ω and W_e have been proposed in the literature. When W is the Dirac-delta function, c_e results in a local quantity, which has been found to be highly fluctuating in space, thus violating one of the assumptions on which the Germano procedure is based. A remedy is to use directions of homogeneity, when available, that translate the integrals $I_{\Lambda\Upsilon}$ and $I_{\Upsilon\Upsilon}$ into spatial averages (either in volume, planes or lines). Alternatively, a Lagrangian averaging procedure (proposed for incompressible flows by Meneveau *et al.* 1996) uses a particular combination of temporal domain Ω and a weighting function $W(t)$ following fluid particle trajectories, which makes it applicable to any flow type, regardless of inhomogeneity. The extension of the Lagrangian averaging procedure to compressible flows is developed in Appendix A.

In the canonical shock-turbulence interaction flow, transverse planes parallel to the nominal shock can be approximately considered homogeneous. As the intensity of the incoming turbulence increases, the shock becomes more corrugated or even broken, and the approximation of homogeneity in transverse planes may lead to incorrect results in the computation of the model coefficients near the shock, making the use of Lagrangian averaging advantageous. In this study, the two averaging strategies (on transverse planes and along Lagrangian trajectories) will be considered. In the Lagrangian averaging, the initialization of the model coefficients (C_I, C and C/Pr_t) is done with the values obtained from an independent LES of decaying isotropic turbulence with a pure eddy-diffusivity model and both Smagorinsky and Vreman eddy diffusivities, resulting in $(0.0768, 0.0256, 0.0256)$ and $(0.074, 0.0164, 0.0234)$ for each type of eddy diffusivity, respectively.

In this study, the discrete test-filter $\widehat{f}_i = \sum_{k=-N}^{N} a_k f_{i+k}$ used in the dynamic procedure has coefficients $a_k = (1/4, 1/2, 1/4)$, $N = 1$ and width $\sqrt{6}$, whereas the unknown Favre-filter in the similarity mixed term is approximated by a discrete filter with coefficients $(1/8, 3/4, 1/8)$ and width $\sqrt{3}$ (based on the second-order moment of the filter kernel).

3.2. *Stretched-vortex model*

The stretched-vortex model, originally developed for incompressible flows in Misra & Pullin (1997) and extended to compressible flows in Kosović *et al.* (2002), is a structural model which assumes the subgrid motion in each cell to be produced by a superposition of nearly axisymmetric vortices, whose ensemble dynamics can be characterized by a vortex aligned with the unit vector e^v, modeled through a delta-function probability density function (pdf). The SGS stresses are then defined as $\tau_{ij}^S = \overline{\rho}K(\delta_{ij} - e_i^v e_j^v)$, where $\overline{\rho}K = \overline{\rho}\int_{k_c}^{\infty} E(k)\mathrm{d}k = \tau_{kk}^S/2$ is the SGS turbulent kinetic energy ($k_c = \pi/\Delta$ is the cutoff wavenumber), which is estimated assuming the form of the energy spectrum proposed by Lundgren (1982). The SGS heat flux is modeled by means of the SGS scalar flux model (Pullin 2000) as $q_i^S = (\Delta/2)\sqrt{K}(\delta_{ij} - e_i^v e_j^v)\partial\widetilde{T}/\partial x_j$.

A vortex orientation model has to be specified for $\mathbf{e}^v$ to be defined. Two different models are considered in this study: the first, denoted V1, assumes the vortex to be aligned with the most extensional eigenvector, $\widetilde{\mathbf{e}}_3$, of the resolved strain-rate tensor, $\widetilde{S}_{ij}$, associated with the eigenvalue λ_3; the second, V2, uses a local pdf of the form $P(\mathbf{e}^v) = \theta\delta(\mathbf{e}^v|\widetilde{\mathbf{e}}_3) + (1-\theta)\delta(\mathbf{e}^v|\widetilde{\mathbf{e}}_\omega)$, where $\widetilde{\mathbf{e}}_\omega$ is the unit vector of the resolved vorticity (ω_i), $\delta(\mathbf{m}|\mathbf{n})$ is the delta-function probability density that $\mathbf{m}$ is aligned with $\mathbf{n}$, and θ is the fraction of SGS vortices aligned with $\widetilde{\mathbf{e}}_3$, given by the ansatz $\theta = \lambda_3/(\lambda_3 + \sqrt{\widetilde{\omega}_i\widetilde{\omega}_i})$.

4. Conditional application of SGS models in a hybrid methodology

As discussed in Section 2, a hybrid approach that applies a WENO scheme in regions near shock waves and a central-difference scheme elsewhere is used. To capture shock waves, WENO schemes add excessive numerical dissipation, damping the turbulence in those regions, which affects the post-shock turbulence (see Larsson 2010). Further application of an SGS model in WENO regions can result in an overly dissipative combination, which can be avoided by conditioning the application of the SGS model to flow regions where WENO is not active. The same WENO sensor is used by the SGS model to set the modeled SGS terms to zero. This is done prior to the calculation of the divergence of those SGS terms, as they appear in the equations of motion, ensuring conservation of momentum and total energy. Results of LES with and without this conditional SGS application in use will be compared in Section 5. Note that this technique is independent of the SGS model in use.

When Lagrangian averaging is used for eddy-diffusivity models, regions where the model is not active simply transport the model coefficients from the previous point of the fluid particle trajectory by setting $\epsilon_{AB} = 0$ in (A 4), and thus, across the shock wave region. A more elaborate approach could incorporate theoretical elements of linear interaction analysis (LIA) or rapid distortion theory (RDT) to modify the model coefficients across the shock wave, instead of transporting them from the upstream side to the downstream (which assumes the same level of turbulence on both sides). We use the latter approach for its simplicity. Note also that the values of the coefficients will adjust dynamically to the actual new levels of turbulence found downstream.

5. Results

LES results are compared with filtered DNS data through streamwise profiles obtained from averaged statistics in time and across transverse planes for two different mean Mach numbers of the incoming flow ($M = 1.5$, 3.5). LES are performed on an isotropic grid G1 with 98×64^2 points, for which the LES cut-off is still separated from the large scales. For the $M = 1.5$ case we also present results for a second grid G2 which doubles the resolution in the streamwise direction (i.e., 196×64^2 points). The DNS used for comparison was performed on a grid with 2234×1024^2 points, stretched in the streamwise direction to allow a three-fold increase of the resolution at and behind the shock and later filtered to each LES resolution.

Mean flow quantities obtained from the LES show good agreement with the filtered DNS results and are not presented. We focus on turbulence-related quantities, namely the streamwise and transverse Reynolds stresses normalized with their values upstream of the shock, R_{xx}/R^u_{xx} and R_{yy}/R^u_{yy}, their anisotropy, the turbulent kinetic energy, TKE, and the SGS dissipation, $-\tau^S_{ij}\widetilde{S}_{ij}$. Figures 1, 2 and 4 contain plots of these quantities, for the implemented models specified in Table 2. Filtered DNS and no-model LES are included for comparison. We plot the subdomain $x - x_s \in [-1.25, 5]$, which excludes the sponge region near the outlet and part of the upstream region farther from the shock.

For $M = 1.5$ and grid G1, the shape of the profile of normalized streamwise Reynolds stress, R_{xx}/R^u_{xx} (Figure 1a), is well captured by most models, although the amplification level across the shock is overestimated by all models. Mixed models with Vreman's eddy-diffusivity present the best agreement with filtered DNS data and lead to rates of change upstream and downstream of the shock which are closest to the filtered DNS results. The selection of the mixed term in use has a small effect on the result, for this particular flow.

ID	Class	Mixed term	Eddy-diffusivity/ orientation model	Averaging	Line style
MNSP	Mixed	None	Smagorinsky	Transverse planes	Red solid
MGSP	Mixed	Gradient	Smagorinsky	Transverse planes	Red dashed
MSSP	Mixed	Similarity	Smagorinsky	Transverse planes	Red dotted
MNSL	Mixed	None	Smagorinsky	Lagrangian	Green solid
MGSL	Mixed	Gradient	Smagorinsky	Lagrangian	Green dotted
MSSL	Mixed	Similarity	Smagorinsky	Lagrangian	Green dashed
MNVP	Mixed	None	Vreman	Transverse planes	Brown solid
MGVP	Mixed	Gradient	Vreman	Transverse planes	Brown dashed
MSVP	Mixed	Similarity	Vreman	Transverse planes	Brown dotted
MNVL	Mixed	None	Vreman	Lagrangian	Blue solid
MGVL	Mixed	Gradient	Vreman	Lagrangian	Blue dashed
MSVL	Mixed	Similarity	Vreman	Lagrangian	Blue dotted
SPM	Stretched-vortex	N/A	Extensional (V1)	Transverse circle	Cyan solid
SPL	Stretched-vortex	N/A	Local pdf (V2)	Transverse circle	Cyan dashed

TABLE 2. Implemented models.

The stretched-vortex model performs better with the orientation model V1, providing a peak value immediately downstream of the shock closest to the filtered DNS, although the subsequent rate of decay is underpredicted (also upstream of the shock).

Results for the normalized transverse Reynolds stress, R_{yy}/R^u_{yy}, show (Figures 1b) worse agreement than for R_{xx}/R^u_{xx}. The best agreement with filtered DNS is provided by mixed models with Vreman's eddy-diffusivity and Lagrangian averaging, even though the value immediately downstream of the shock is still underpredicted. Upstream of the shock, the decay rate of R_{yy} is also best captured by those models. Note that other models result in R_{yy} that are not monotonically decreasing downstream of the shock.

The normalized turbulent kinetic energy, TKE/TKE^u, shown in Figures 1c, reflects a consistent underprediction of the amplification occurring immediately after the shock, due to the underprediction of R_{yy}. This is compensated by the overprediction of R_{xx} farther downstream, recovering the proper rate of decay. Models with Vreman's eddy-diffusivity provide the best results.

Overprediction of R_{xx} and underprediction of R_{yy} downstream of the shock, described above for all models, result in levels of anisotropy (R_{yy}/R_{xx}) that differ significantly from the filtered DNS data (Figure 1d). Note that even upstream of the shock there is a lack of agreement. As before, models with Vreman's eddy-diffusivity show better results.

Figure 2 shows results obtained by doubling the resolution in the streamwise coordinate (grid G2), for $M = 1.5$. The finer streamwise grid has the greatest impact in R_{yy} which reproduces the results of the filtered DNS more accurately (Figure 2b) than for grid G1, particularly in the region immediately downstream of the shock. This could indicate that high streamwise-wavenumbers contain motions primarily leading to transverse Reynolds stresses. As a result, the profiles of TKE and Reynolds stress anisotropy (Figure 2c,d) follow the filtered DNS results more closely. Again, the best results are obtained with Vreman's eddy-diffusivity models. Note, nonetheless, that a Vreman's eddy-diffusivity model with similarity mixed term and transverse plane averaging results in a wrong prediction of turbulence quantities for $x - x_s > 2$, which was traced back to changes in the trend of eddy-diffusivity model coefficients and is presently under further investigation.

Figure 3 shows streamwise velocity spectra computed on transverse planes at four

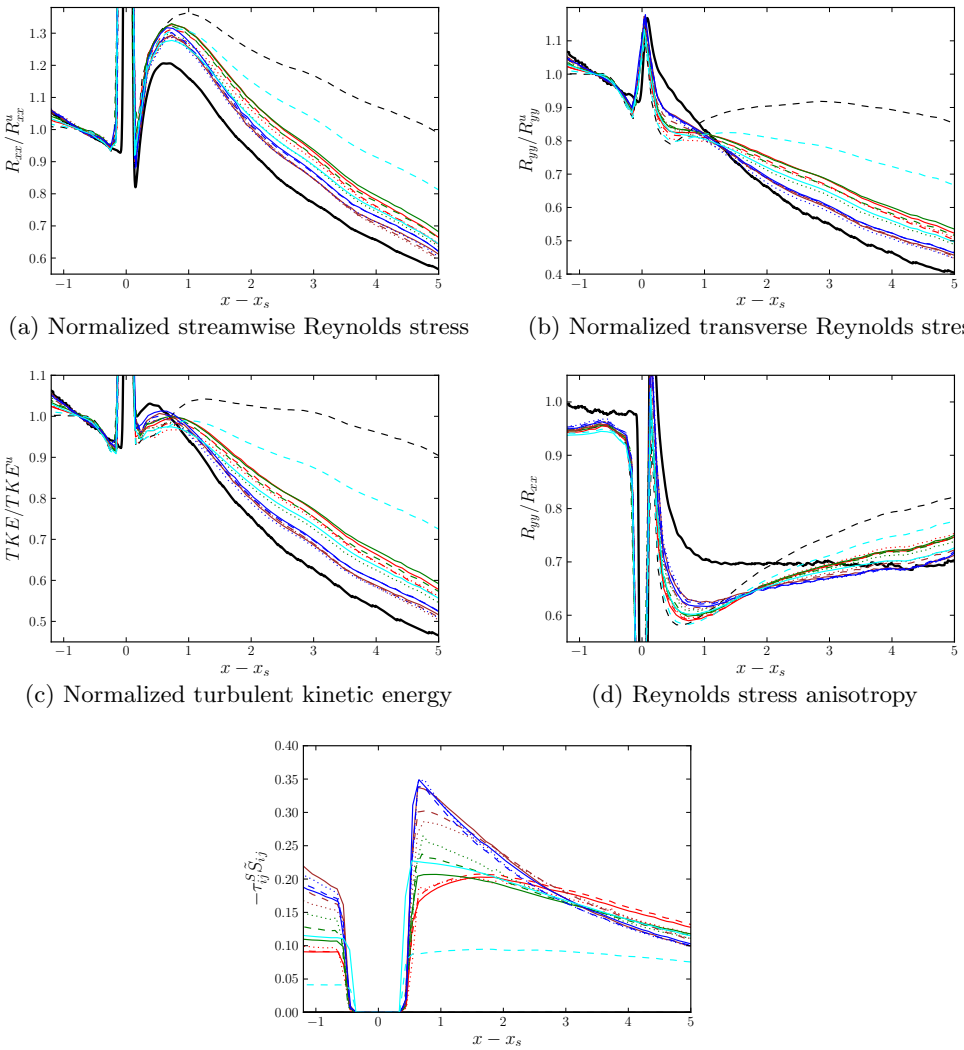

(a) Normalized streamwise Reynolds stress

(b) Normalized transverse Reynolds stress

(c) Normalized turbulent kinetic energy

(d) Reynolds stress anisotropy

(e) Subgrid-scale dissipation

FIGURE 1. LES results for $M = 1.5$ and grid G1. Filtered DNS, solid black; no-model LES, dashed black. See Table 2 for SGS-LES line styles.

streamwise locations relative to the average shock position ($x - x_s = -1.0, 1.0, 3.0, 5.0$), for all LES models on grid G1, compared to filtered DNS and no-model LES (which acts as an upper bound). Upstream of the shock, Vreman's eddy-diffusivity models appear to dissipate slightly more energy than that required in the resolved part of the inertial range, particularly when Lagrangian averaging is used. After the shock, an energy transfer to the low-wavenumber part of the spectra occurs for all models. Pile-up of the spectra at high wavenumbers is noticeable at $x - x_s = 1.0$ for most models, increasing downstream, except for mixed Vreman's eddy-diffusivity models with Lagrangian averaging and the pure Vreman's eddy-diffusivity model with transverse plane averaging, whose spectra remain close to the filtered DNS and below them for the majority of wavenumbers.

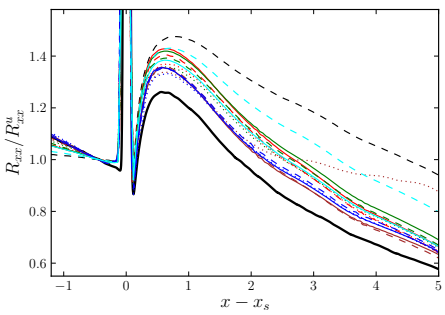

(a) Normalized streamwise Reynolds stress

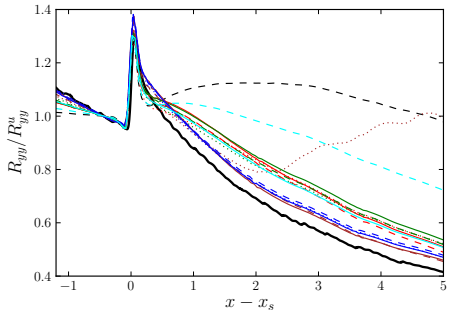

(b) Normalized transverse Reynolds stress

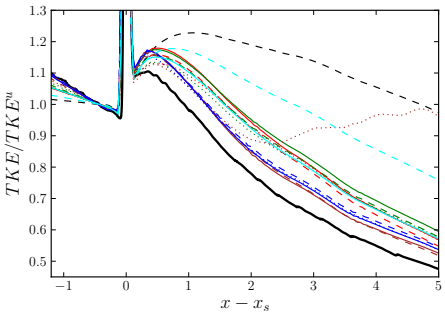

(c) Normalized turbulent kinetic energy

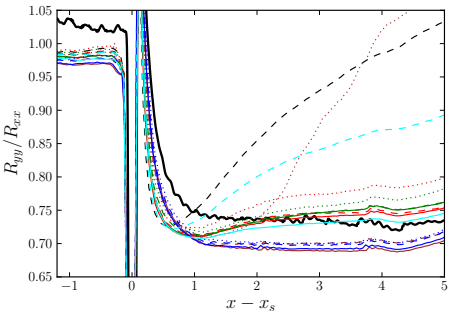

(d) Reynolds stress anisotropy

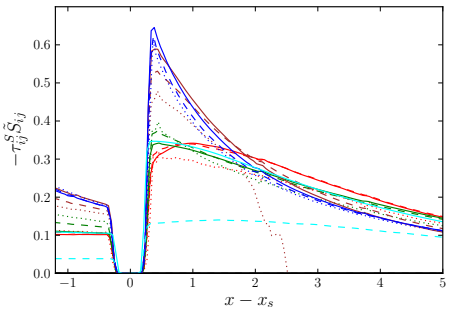

(e) Subgrid-scale dissipation

FIGURE 2. LES results for $M = 1.5$ and grid G2. Filtered DNS, solid black; no-model LES, dashed black. See Table 2 for SGS-LES line styles.

Figure 4 shows streamwise profiles of turbulence-related quantities for the case with $M = 3.5$ and grid G1. Errors in the amplification of normal Reynolds stresses increase with respect to the $M = 1.5$ case: R_{xx}/R^u_{xx} is more overpredicted and R_{yy}/R^u_{yy} is more underpredicted immediately downstream of the shock. These two effects cancel out in the TKE/TKE^u, obtaining reasonable agreement with filtered DNS at both Mach numbers, but add up, on the other hand, in the prediction of Reynolds stress anisotropy, which worsens for the larger Mach number. Consistently with the lower M case, the best results are provided by Vreman's eddy-diffusivity models. Note the increase in SGS dissipation immediately downstream of the shock provided by the Lagrangian averaging compared to the transverse plane averaging from $M = 1.5$ to $M = 3.5$ (Figures 1e and 4e).

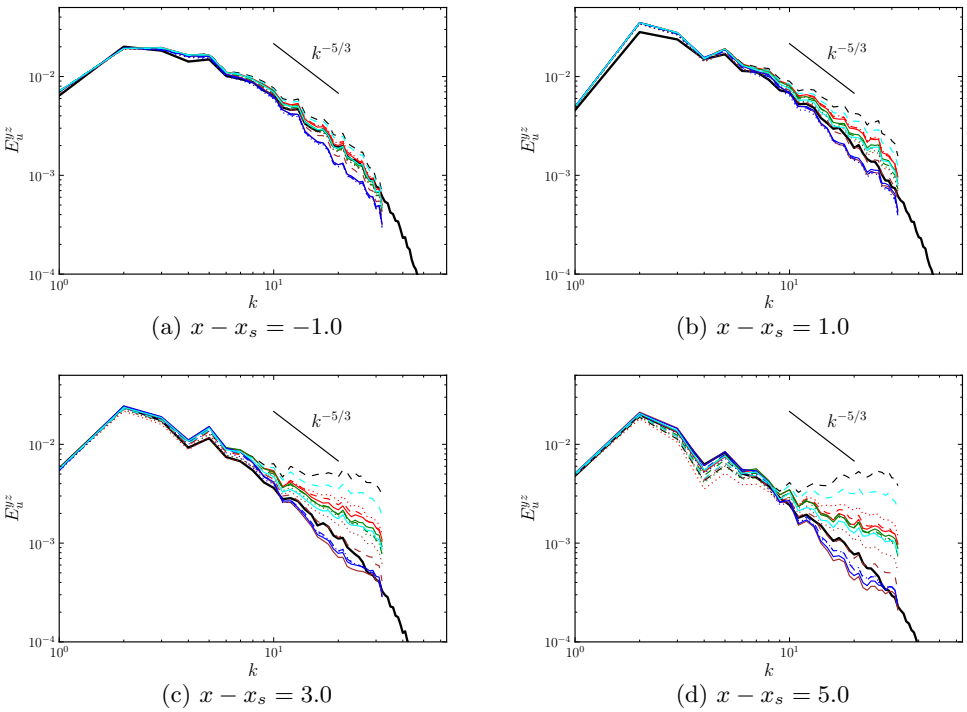

(a) $x - x_s = -1.0$ (b) $x - x_s = 1.0$

(c) $x - x_s = 3.0$ (d) $x - x_s = 5.0$

FIGURE 3. Streamwise velocity spectra obtained from LES with different models compared to filtered DNS for $M = 1.5$ and grid G1 at four locations relative to the average shock position. Filtered DNS is plotted in solid black and LES with no model in dashed black. The line styles corresponding to the LES with the different implemented models are specified in Table 2.

5.1. *Impact of the order/directionality of WENO scheme and conditional SGS*

The results presented so far were obtained with a seventh-order accurate WENO scheme applied only in the streamwise direction near the shock. In addition, SGS models were not applied in regions where WENO was active. This subsection evaluates the effect of 1) modifying the order of accuracy of the WENO scheme, 2) applying WENO also in the transverse directions (common in more complex flows where the shock orientation is unknown or might involve multiple coordinate axes), and 3) applying SGS everywhere.

Figure 5 shows turbulence-related quantities for LES performed with the Lagrangian-averaged dynamic Vreman's eddy-diffusivity model (MNVL) and different variants of WENO schemes, directionality and conditional SGS application. The order of accuracy of the WENO scheme plays a decisive role in the amplification of turbulence across the shock and its downstream evolution, at this grid resolution. The results obtained with a third-order WENO compare poorly with filtered DNS: in particular, instead of the expected amplification of R_{yy} after the shock and its monotonic decrease downstream, their values are significantly reduced immediately after the shock, remaining almost constant farther downstream. Fifth-order WENO improves substantially the results: even though there is still no amplification of R_{yy} after the shock, the monotonic decrease downstream is better reflected, approaching the correct value at $x - x_s = 5$. R_{xx} is also significantly improved. Seventh-order WENO provides better results, particularly for R_{yy} and TKE. These three cases applied WENO only in the streamwise coordinate direction.

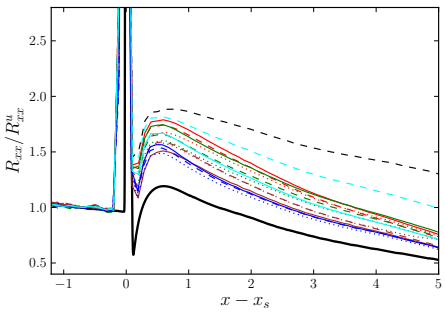

(a) Normalized streamwise Reynolds stress

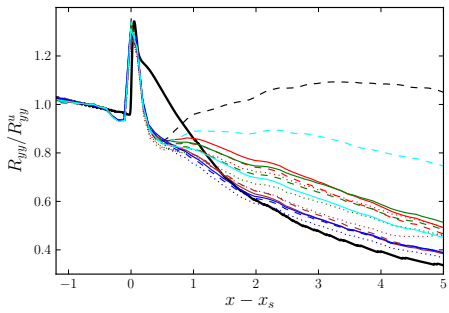

(b) Normalized transverse Reynolds stress

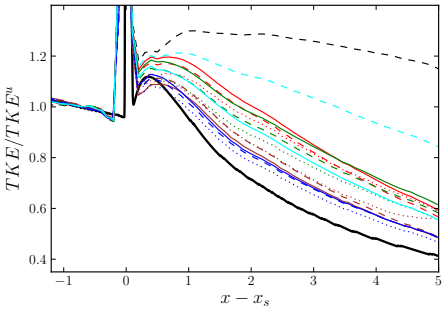

(c) Normalized turbulent kinetic energy

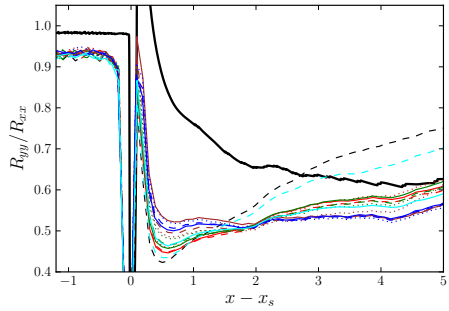

(d) Reynolds stress anisotropy

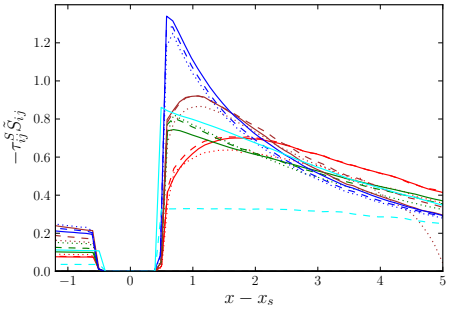

(e) Subgrid-scale dissipation

FIGURE 4. LES results for $M = 3.5$ and grid G1. Filtered DNS, solid black; no-model LES, dashed black. See Table 2 for SGS-LES line styles.

The additional damping obtained when seventh-order WENO is applied in all three coordinate directions (dash-dotted line in Figure 5), instead of only in the streamwise direction, is more noticeable for R_{xx} than for R_{yy}. The transverse Reynolds stress and TKE are comparable to those obtained with a fifth-order WENO applied only in the streamwise direction, although the decay rate farther downstream is more underpredicted.

When the SGS model is applied everywhere, the extra SGS dissipation added in WENO regions (see dotted line in Figure 5e) considerably damps the turbulence across the shock. R_{xx} levels are comparable to those obtained with a third-order WENO, whereas R_{yy} lies between a third- and a fifth-order WENO. The rate of change downstream follows the filtered DNS results, but the absolute values are considerably lower.

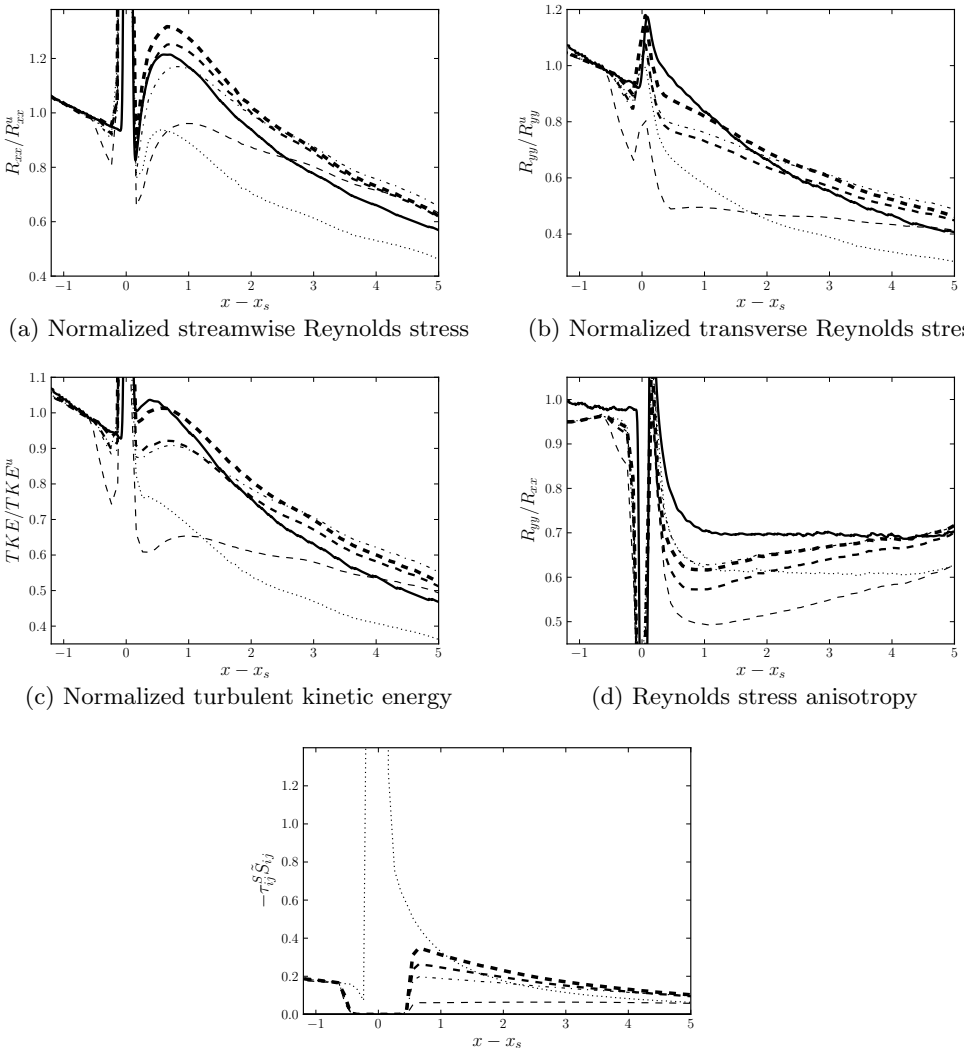

(a) Normalized streamwise Reynolds stress

(b) Normalized transverse Reynolds stress

(c) Normalized turbulent kinetic energy

(d) Reynolds stress anisotropy

(e) Subgrid-scale dissipation

FIGURE 5. LES and filtered DNS results for $M = 1.5$ and grid G1 with the Lagrangian-averaged dynamic Vreman's eddy-diffusivity model. Filtered DNS, solid line; LES with third-, fifth- and seventh-order WENO schemes applied only in the streamwise direction near shocks and conditional SGS (only applied where WENO is not active) are plotted in dashed lines of thickness increasing with the WENO order of accuracy; LES with seventh-order WENO scheme applied in the three coordinate directions and conditional SGS is plotted in dash-dotted line; LES with seventh-order WENO scheme and SGS model applied everywhere is plotted in dotted line.

6. Conclusions and future work

The performance of several SGS models in LES of canonical shock-turbulence interaction has been evaluated at two different flow conditions, by comparing turbulence-related quantities with filtered DNS data. Vreman's eddy diffusivity was found to improve the results over the traditional Smagorinsky's eddy diffusivity. The application of the Lagrangian averaging procedure to compressible flows also improves the results for the

higher Mach number under consideration and has the advantage of being applicable to inhomogeneous flows. The inclusion of gradient or similarity mixed terms had a relatively small effect in the results for this type of flow, when compared with a purely eddy-diffusivity model. Grid refinement in the shock-normal direction mainly improves the prediction of transverse Reynolds stresses.

Conditional application of SGS models only in regions where WENO scheme is not active has been proposed to avoid adding extra SGS dissipation where the expected numerical dissipation is already high. This technique considerably improves the results. The impact of the order of accuracy of WENO schemes and the directions in which WENO is applied was evaluated for one of the SGS models. Third-order WENO resulted in a poor agreement with filtered DNS data, whereas fifth-order WENO improved considerably the results. The amplification of transverse Reynolds stress immediately downstream of the shock required seventh-order WENO being applied only in the streamwise coordinate to be captured in the LES. When WENO is applied in the three coordinates, the extra numerical dissipation introduced damps substantially the turbulence quantities. The necessity of a high-order WENO scheme applied only in the shock-normal direction poses a significant challenge for accurate simulations of more complex flows in which the use of low-order WENO applied in multiple directions might be required. The effect of grid resolution, Mach number and WENO order in the errors of turbulence amplification across the shock was found in qualitative agreement with the predictions of Larsson (2010).

Future work involves the evaluation of other flow parameters, such as the turbulent Mach number, in the performance of the SGS models as well as the application of the implemented models to more complex flows involving shock-turbulence interaction, such as the shock-boundary layer interaction problem.

Acknowledgments

Financial support has been provided by the Department of Energy under the SciDAC program. I.B-M is grateful to Dr. Daniel K. Chung for providing the subroutines that are the basis of our stretched-vortex SGS model implementation and to Dr. Olaf Marxen for his valuable comments and remarks on a preliminary version of this manuscript.

Appendix A. Lagrangian averaging procedure for compressible flows

In this appendix, the Lagrangian averaging procedure developed by Meneveau *et al.* (1996) for incompressible flows is extended for its application to compressible SGS models, by adding two relaxation-transport equations for each extra model coefficient and redefining the relaxation time scales appropriately. The derivation of the relaxation transport equations follows Meneveau *et al.* (1996) directly and is reproduced here for completeness. The starting point is the expression for the model coefficient obtained by the least-squares minimization procedure (see Section 3.1): $c_e(\mathbf{x},t) = I_{\Lambda\Upsilon}/I_{\Upsilon\Upsilon}$, where the integrals

$$I_{AB}(\mathbf{x},t) = \int_{-\infty}^{t} A(\mathbf{s}(t'),t')B(\mathbf{s}(t'),t')W_e(t-t')\mathrm{d}t' \tag{A 1}$$

are now defined along fluid particle trajectories: $\mathbf{s}(t') = \mathbf{x} - \int_{t'}^{t} \widetilde{\mathbf{u}}(\mathbf{s}(t''),t'')\mathrm{d}t''$. By choosing an exponentially decaying weighting function $W_e(t-t') = (1/\tau_e)\exp[-(t-t')/\tau_e]$, with

a relaxation time τ_e, the material derivative of I_{AB} adopts the simple form

$$\frac{\mathrm{D}I_{AB}}{\mathrm{D}t} = \frac{\partial I_{AB}}{\partial t} + \widetilde{\mathbf{u}} \cdot \nabla I_{AB} = \frac{1}{\tau_e}(AB - I_{AB}), \tag{A 2}$$

where Leibniz's rule for differentiation under the integral sign has been applied. Thus, the calculation of I_{AB} through the integral in (A 1) is substituted for solving the differential equation (A 2). A semi-backward Euler method is used between time steps t_n and t_{n+1}, denoted by the superscripts n and $n+1$, respectively, with the Lagrangian approach for computing the position of the fluid particle at t_n:

$$\frac{I_{AB}^{n+1}(\mathbf{x}) - I_{AB}^{n}(\mathbf{x} - \widetilde{\mathbf{u}}^n \Delta t)}{\Delta t} = \frac{1}{\tau_e^n}[A^{n+1}(\mathbf{x})B^{n+1}(\mathbf{x}) - I_{AB}^{n+1}], \tag{A 3}$$

which leads to

$$I_{AB}^{n+1}(\mathbf{x}) = H_{AB}[\epsilon_{AB}A^{n+1}(\mathbf{x})B^{n+1}(\mathbf{x}) + (1-\epsilon_{AB})I_{AB}^{n}(\mathbf{x} - \widetilde{\mathbf{u}}^n \Delta t)], \tag{A 4}$$

where $\epsilon_{AB} = (\Delta t/\tau_e^n)/[1+(\Delta t/\tau_e^n)]$, $H_{AB}(\theta) = \{\theta, \text{if } A = B; R(\theta), \text{if } A \neq B\}$ and $R(\theta) = \{0, \text{if } \theta < 0; \theta, \text{if } \theta \geq 0\}$, needed to guarantee that the solution is real.

The relaxation time τ_e controls the time scale of the Lagrangian averaging. Following Meneveau *et al.* (1996), τ_e is chosen to depend on the $I_{\Lambda\Upsilon}$ and $I_{\Upsilon\Upsilon}$ Lagrangian averages. Note that (A 2) was derived assuming that τ_e is constant, which is better approximated by choosing a τ_e that does not depend on local, possibly high-fluctuating variables. For the three model coefficients considered in this study (C_I, C and C/Pr_t), dimensional analysis of their associated $I_{\Lambda\Upsilon}$ and $I_{\Upsilon\Upsilon}$ yields $\tau_e^{C_I} \propto \Delta\sqrt{\overline{\rho}}/(I_{\Lambda\Upsilon}^{C_I} I_{\Upsilon\Upsilon}^{C_I})^{1/8}$, $\tau_e^{C} \propto \Delta\sqrt{\overline{\rho}}/(I_{\Lambda\Upsilon}^{C} I_{\Upsilon\Upsilon}^{C})^{1/8}$ and $\tau_e^{C/Pr_t} \propto \Delta\overline{\rho}\widetilde{T}/(I_{\Lambda\Upsilon}^{C/Pr_t} I_{\Upsilon\Upsilon}^{C/Pr_t})^{1/4}$. The constant of proportionality of $\mathcal{O}(1)$ is chosen as $3/2$ in all cases (see Meneveau *et al.* 1996, for a sensitivity analysis on this parameter performed for incompressible fully-developed channel flow). Initial/boundary conditions for the relaxation-transport equations are constructed, for each model coefficient, as $I_{\Lambda\Upsilon}^0 = c_e^{\mathrm{iso}}\,[\Upsilon\Upsilon]^0$, $I_{\Upsilon\Upsilon}^0 = [\Upsilon\Upsilon]^0$, to provide the expected model coefficient for isotropic turbulence, c_e^{iso}.

REFERENCES

Agui, J. H., Briassulis, G. & Andreopoulos, Y. 2005 Studies of interactions of a propagating shock wave with decaying grid turbulence: velocity and vorticity fields. *J. Fluid Mech.* **524**, 143–195.

Barre, S., Alem, D. & Bonnet, J. P. 1996 Experimental study of a normal shock/homogeneous turbulence interaction. *AIAA J.* **34**, 968–974.

Bermejo-Moreno, I. 2009 Subgrid-scale modeling of shock-turbulence interaction for large-eddy simulations. In *Annu. Res. Briefs, Center for Turbulence Research*, pp. 247–259.

Ducros, F., Ferrand, V., Nicoud, F., Weber, C., Darracq, D., Gacherieu, C. & Poinsot, T. 1999 Large-eddy simulation of the shock/turbulence interaction. *J. Comput. Phys.* **152**, 517–549.

Ducros, F., Laporte, F., Souleres, T. & Guinot, V. 2000 High-order fluxes for conservative skew-symmetric-like schemes in structures meshes: Application to compressible flows. *J. Comput. Phys.* **161**, 114.

Germano, M., Piomelli, U., Moin, P. & Cabot, W. H. 1991 A dynamic subgrid-scale eddy viscosity model. *Phys. Fluids A* **3**, 1760–1765.

Hannappel, R. & Friedrich, R. 1995 Direct numerical simulation of a Mach 2 shock interacting with isotropic turbulence. *Appl. Sci. Research* **54**, 205–221.

Hesselink, L. & Sturtevant, B. 1988 Propagation of weak shocks through a random medium. *J. Fluid Mech.* **196**, 513–553.

Jacquin, L., Cambon, C. & Blin, E. 1993 Turbulence amplification by a shock wave and rapid distorsion theory. *Phys. Fluids A* **5**, 2539–2550.

Keller, J. & Merzkirch, W. 1990 Interaction of a normal shock wave with a compressible turbulent flow. *Experiments in Fluids* **8**, 241–248.

Kosović, B., Pullin, D. I. & Samtaney, R. 2002 Subgrid-scale modeling for large-eddy simulations of compressible turbulence. *Phys. Fluids* **14**, 1511–1522.

Larsson, J. 2010 Effect of shock-capturing errors on turbulence statistics. *AIAA J.* **48(7)**, 1554–1557.

Larsson, J. & Lele, S. K. 2009 Direct numerical simulation of canonical shock/turbulence interaction. *Phys. Fluids* **21**, 126101.

Lee, S. 1992 Large eddy simulations of shock turbulence interaction. In *Annu. Res. Briefs, Center for Turbulence Research*, pp. 73–84.

Lee, S., Lele, S. K. & Moin, P. 1992 Direct numerical simulation and analysis of shock turbulence interaction. *AIAA* .

Lee, S., Lele, S. K. & Moin, P. 1993 Direct numerical simulation of isotropic turbulence interacting with a weak shock wave. *J. Fluid Mech.* **251**, 533–562.

Lee, S., Lele, S. K. & Moin, P. 1997 Interaction of isotropic turbulence with shock waves: effect of shock strength. *J. Fluid Mech.* **340**, 225–247.

Lele, S. K. 1992 Shock-jump relations in a turbulent flow. *Phys. Fluids A* **4**, 2900–2905.

Lilly, D. K. 1992 A proposed modification of the Germano subgrid-scale closure method. *Phys. Fluids A* **4** (3), 633–635.

Lundgren, T. S. 1982 Strained spiral vortex model for turbulent fine structure. *Phys. Fluids* **12**, 2193.

Mahesh, K., Lele, S. K. & Moin, P. 1997 The influence of entropy fluctuations on the interaction of turbulence with a shock wave. *J. Fluid Mech.* **334**, 353–379.

Meneveau, C., Lund, T. S. & Cabot, W. H. 1996 A Lagrangian dynamic subgrid-scale model of turbulence. *J. Fluid Mech.* **319**, 353–385.

Misra, A. & Pullin, D. I. 1997 A vortex-based subgrid stress model for large-eddy simulation. *Phys. Fluids* **9**, 2443–2454.

Pullin, D. I. 2000 A vortex-based model for the subgrid flux of a passive scalar. *Phys. Fluids* **12**, 2311–2319.

Ribner, H. S. 1953 Convection of a pattern of vorticity through a shock wave. *NACA Rep.* **1164**.

Smagorinsky, J. 1963 General circulation experiments with the primitive equations 1. the basic experiment. *Mon. Weather Rev.* **91**, 99–164.

Vreman, A. W. 2004 An eddy-viscosity subgrid-scale model for turbulent shear flow: Algebraic theory and applications. *Phys. Fluids* **16** (10), 3670–3681.

Wouchuk, J. G., Huete Ruiz de Lira, C. & Velikovich, A. 2009 Analytical linear theory for the interaction of a planar shock wave with an isotropic turbulent vorticity field. *Phys. Rev. E* **79**, 066315.